H2 production from the photocatalytic reforming of ethylene glycol: Effect of TiO2 crystalline phase on photo-oxidation mechanism

H₂ production from the photocatalytic reforming of ethylene glycol: Effect of TiO₂ crystalline phase on photo-oxidation mechanism

Luke Roebuck [a,*], Helen Daly [a], Lan Lan [a], Joseph Parker [b], Angus Gostick [a], Nathan Skillen [c], Sarah J. Haigh [b], Marta Falkowska [a], Christopher Hardacre [a,*]

[a] *Department of Chemical Engineering, School of Engineering, The University of Manchester, M13 9PL, United Kingdom*
[b] *Department of Materials, School of Natural Sciences, University of Manchester, Manchester M13 9PL, United Kingdom*
[c] *School of Chemistry and Chemical Engineering, Queen's University Belfast, Belfast BT9 5AG, United Kingdom*

ARTICLE INFO

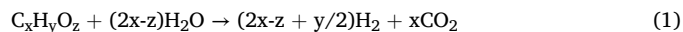## ABSTRACT

In this work, the mechanism of H₂ production from ethylene glycol as a model compound for photoreforming over platinized TiO₂ is presented with particular focus on the effect of the TiO₂ polymorph. It was found that Pt/anatase and Pt/anatase:rutile (P25) had similar H₂ production activities and both catalysts followed an indirect oxidation pathway where ethylene glycol was oxidised via hydroxyl radicals to glycolaldehyde. In contrast, Pt/rutile primarily oxidised ethylene glycol directly into formaldehyde. The formaldehyde was unable to react further, which significantly reduced the formation of hydrogen despite similar conversion of ethylene glycol compared with the other supports used. We propose that these differences are due to different adsorption behaviour and hole transfer mechanism on the different TiO₂ crystalline phases. In particular, ethylene glycol complexation on Ti₅c sites on the dominant (110) facet of rutile leads to a direct hole transfer and an oxidative C–C cleavage mechanism prevailing.

1. Introduction

Photocatalytic reforming (photoreforming) involves the use of a semiconductor photocatalyst for the simultaneous oxidation of organic species and hydrogen evolution under anaerobic conditions. Various organic substrates have been investigated as sacrificial agents including alcohols, sugars, biomass, and plastics [1–5]. The organic substrate is oxidised by photogenerated holes or hydroxyl radicals to CO₂ via a series of intermediates. Protons are released during each oxidation step and via water oxidation which are then reduced at reduction sites by photogenerated electrons to form H₂ [6]. The general formula for photoreforming is shown below.

$$C_xH_yO_z + (2x\text{-}z)H_2O \rightarrow (2x\text{-}z + y/2)H_2 + xCO_2 \tag{1}$$

As a route to low energy cost and low or net-zero carbon hydrogen production, photoreforming has attracted much attention in the last decade. In particular, if biomass derivatives are used as the organic substrate, then the technology may be considered carbon–neutral or even carbon-negative if the CO₂ produced is captured and/or further converted to value added products [7]. Furthermore, photoreforming may be considered a waste-to-energy technology if pollutants or waste carbon-based materials are used [8]. In this work ethylene glycol has been investigated as a substrate for photoreforming. Vicinal diol or glycol groups are ubiquitous in bioderived compounds and, therefore, the study of ethylene glycol also serves as a tool to gain mechanistic understanding that may be applied to more complex biomass photoreforming substrates. Moreover, ethylene glycol may exist as a waste or pollutant material. It is a high production volume chemical and may be present as a waste product in industrial processes such as chemical recycling of polyethylene terephthalate (PET) when its separation from water is not economically viable [9,10]. As a pollutant, for example, it is also present in run-off from airplane and runway de-icing processes. Issues arise from ethylene glycol's toxicity and potential environmental damaging effects, therefore, when present in effluents it should be eliminated [11,12].

TiO₂ has been the most widely employed photocatalyst in photoreforming due to its stability, earth abundance, cost and ease of synthesis, and most importantly its suitable valence and conduction band positions to facilitate H⁺ reduction and oxidation of the organic substrate [13]. Two main polymorphs of TiO₂ have found application in

photocatalysis: anatase and rutile. Anatase is often considered to be the most active phase;[14] however, the reasons for this are complex. For example, it has been reported that the anatase surface has a greater degree of hydroxylation leading to greater quantities of oxidising hydroxyl radicals [15]. Anatase is also proposed to have better transport of photogenerated charge carriers to the catalyst surface [16]. Mixed phase catalysts such as Evonik® P25 have become the benchmark in the field [17] which is reportedly due to the enhanced separation of the photo-generated charge carriers at the anatase:rutile phase heterojunction. However, this explanation has been challenged in a number of studies [17–19]. Charge carrier dynamics are not always the most important factor in determining overall performance, particularly when more complex substrates are employed. Various reports have in fact shown rutile based catalysts to be more effective when particular substrates are used indicating that the oxidation mechanisms are key to determining overall activity [3,20].

Photo-oxidation of mono- and poly-ols over TiO_2 in anaerobic conditions occurs either by direct hole transfer following chemisorption or by reaction with photogenerated hydroxyl radicals. Using glycerol as a probe molecule, Maurino et al. have investigated the effects of these two mechanisms. It was shown that oxidation by the direct hole transfer usually leads to cleavage of the C–C bond adjacent to the hydroxyl group. In contrast, oxidation via hydroxyl radicals is responsible for oxidation without cleavage to smaller chain species. Maslova et al. and Chong et al. have recently demonstrated that rutile content in TiO_2 increased the amount of shorter chain products [20,21]. This indicates that complexation sites and, therefore, oxidation by direct hole-transfer on rutile may be more prevalent than on anatase. This difference in mechanism meant that the rutile catalysts produced H_2 at greater rates as the glycerol could be mineralised fully in fewer oxidation steps. This has also been observed in glucose photoreforming where C–C cleavage produces formic acid resulting in greater H_2 evolution [3,22]. Herein, we investigate the effect of the TiO_2 crystalline phase on the oxidation mechanism using ethylene glycol as a probe molecule.

2. Experimental

2.1. Chemicals & materials

15 wt% $Pt(NO_3)_4$ precursor solution, hydrochloric acid (37 %), and nitric acid (70 %), were obtained from Alfa Aesar/Thermo Fischer. Anatase (99.7 %), rutile (99.5 %), ethylene glycol (99.8 %), glyco-laldehyde, paraformaldehyde (95 %), acetic acid (99.5 %), platinum standard solution (1000 mg/ml) were purchased from Sigma-Aldrich®. All chemicals were used as received. Commercially available TiO_2 support Aeroxide® P25 was obtained from Evonik. Paraformaldehyde was used to prepare formaldehyde solutions by dissolution in deionised water at 60 °C prior to photoreforming reactions. All other chemicals were used as received with no further treatment. Deionised water (18.2 MΩ) was used for all experiments which was obtained from the Direct-Q 3UV ultrapure water system (Millipore®).

2.2. Catalyst synthesis

Platinum catalysts on the TiO_2 supports were prepared by wet impregnation. Typically, 2 g of catalyst was prepared by dispersing the appropriate quantity of TiO_2 in 20 ml of deionised water and adding dropwise the appropriate amount of $Pt(NO_3)_4$ solution in order to achieve a final platinum loading of 0.2 wt%. This loading has previously shown to be optimal in Pt/TiO_2 photocatalysts [23]. The solutions were then evaporated to dryness over approximately 4 h under magnetic stirring at 60 °C. The resultant catalysts were then dried in a convection oven at 150 °C for 1 h before calcination in static air at 500 °C for 2 h. Finally the catalysts were reduced in pure H_2 (99.99 %, BOC) at 200 °C for 1 h with a 5 °C/h heating rate in a tube furnace.

2.3. Catalyst characterisation

The prepared Pt/TiO_2 catalysts were characterised by powder X-ray Diffraction (XRD), low-temperature N_2 adsorption and Inductively Coupled Plasma Optical Emission Spectroscopy (ICP-OES). The XRD patterns were collected using a Bruker D2 Phaser benchtop diffractometer with a CuK_α (λ = 0.154 nm) radiation source. Measurements were performed over a range of 2θ from 10° to 90° with a step size of 0.02°. N_2 adsorption–desorption measurements were performed at 77 K using a Micromeritics ASAP 2020 surface area analyser to determine the specific surface area of the catalysts using the Brunauer-Emmett-Teller (BET) model. ICP-OES analysis was performed in order to determine the Pt loading. Therein, a 25 mg catalyst sample was dissolved in 12 ml aqua regia (3:1 ratio of HCl and HNO_3) by microwave digestion at 200 °C for 20 min using an ETHOS EASY system. The samples were then measured by an Analytik Jena PlasmaQuant PQ 9000 Elite ICP-OES instrument at three different emission lines corresponding to Pt at 270.2, 283.0 and 299.8 nm. The instrument was calibrated using five Pt standard solutions covering the expected loading range. The dispersion of Pt nanoparticles over the TiO_2 surface of the prepared catalysts was obtained using Scanning Transmission Electron Microscopy (STEM) using a probe-corrected FEI Titan G2 microscope. The microscope was used with a High-Angle Annular Dark Field (HAADF) detector geometry to give Z-contrast. Crystalline phases for the Pt/P25 catalyst were identified by lattice spacing measurements from the acquired TEM images.

2.4. Photoreforming of ethylene glycol using Pt/TiO_2 catalysts.

In a typical photoreforming experiment 40 mg of catalyst was suspended in 40 ml of ethylene glycol/water mixture in a sealed flat-bottomed borosilicate glass reactor (Fig. S1). The reactor was magnetically stirred inside a sealed box to prevent reaction from ambient light and to protect the user from UV exposure. An Ar gas line was positioned in the liquid of the reactor through a septum through the lid of the reactor. Similarly, a gas line out of the headspace of the reactor was fitted to allow for venting of the gas during purging and to allow continuous on-line gaseous sampling at regular time intervals. Prior to each experiment, the reactor was purged with argon for 30 min to remove any dissolved oxygen. The purging was performed under dark conditions in order to check that no thermal reactions had taken place. The reactor was then irradiated using an UV LED array (12 V, SMD3528, λ = 365——375 nm) resulting in an irradiance of 0.028 W/cm^2 on the reactor for 4 h at ambient temperature. The temperature of the reaction was monitored by an internal thermocouple and factored into subsequent gas evolution calculations. Gaseous samples were measured using an Agilent 8860 online gas chromatograph (GC) system equipped with thermal conductivity detector (TCD) and flame ionisation detector (FID) using Porapak Q and HayeSep D columns in series with an Ar carrier gas. Liquid samples were analysed using an Agilent 1220 Infinity II HPLC system with refractive index (RI) and UV-diode array detection (DAD) (λ = 210 nm) using an Aminex HPX-87H column with a 5 mM H_2SO_4 mobile phase.

3. Results & discussion

3.1. Catalyst characterisation

The X-Ray diffraction patterns of each catalyst are shown in Fig. S2. No diffraction peaks associated with Pt^0 or PtO_x were observed indicating that the platinum is well dispersed and/or is below the detection limits of the technique. Pt/anatase and Pt/rutile show the typical diffraction patterns of pure TiO_2 anatase and rutile respectively whereas Pt/P25 catalyst shows diffraction peaks from both phases. The fraction of rutile phase in the catalysts was calculated from the intensities of the anatase (101) and rutile (110) reflections (labelled in Fig. S2) according to previously described methods [24]. It was determined that Pt/P25

contained 19.6 wt% rutile whereas Pt/anatase and Pt/rutile were essentially phase pure. HAADF-STEM images and Pt particle size distributions for are shown in Figs. S3 and S4. All catalysts showed Pt particles with a mean diameter < 1 nm with no particles found to have diameters greater than 5 nm. Slightly larger particles were found on rutile vs anatase which was also found to be true on the mixed phase P25 support. Additionally, some evidence for single atom Pt was observed in each catalyst. Quantitative ICP-OES analysis showed that all catalysts were close to the target platinum loading of 0.2 wt%. BET surface area measurements were determined using low temperature (77 K) N_2 adsorption. The highest surface area was measured for the anatase catalyst at 60.3 m^2/g followed by P25 at 40.4 m^2/g and the lowest for the rutile catalyst at 21.2 m^2/g. The results of the catalyst characterisation are summarised in Table 1 below.

3.2. Photoreforming reactions

3.2.1. Photoreforming of ethylene glycol

During the photoreforming of ethylene glycol (0.3 M), only small quantities of H_2 and CO_2 were produced when no Pt was loaded onto the TiO_2 supports with anatase > P25 > rutile due to poor charge separation of photogenerated charge carriers (Fig. S5). In addition, using the supported Pt catalysts in the absence of a sacrificial agent, i.e. pure water splitting, Pt/P25 and Pt/anatase produced 8 and 4.5 µmol H_2, respectively, after 120 min with Pt/rutile resulting in no H_2 formation (Fig. S5). The H_2 production decreases over time in all cases which has previously been attributed to the build-up of peroxide on the catalyst surface [25]. The low H_2 evolution in these control reactions highlight the importance of both the noble metal and the sacrificial agent acting as electron sinks and hole scavengers, respectively. This is facilitated by presence of the sacrificial agents and the loading of TiO_2 with Pt. The evolution of gaseous phase products formed from the photoreforming of ethylene glycol with Pt/anatase, Pt/rutile, and Pt/P25 catalysts are shown in Fig. 1. The main gaseous products formed as expected are H_2 and CO_2. No CO, CH_4 or higher hydrocarbons were observed, in contrast to previous reports [26]. During these photoreforming experiments Pt/anatase was found to be the most active photocatalyst in terms of H_2 evolution with 1543 µmol H_2 produced after 4 h of irradiation with a quantum efficiency (QE) of 15.9 % followed by Pt/P25 (1142 µmol, QE = 11.7 %) and then Pt/rutile (423 µmol, QE = 4.3 %). However, Pt/P25 had a slightly higher CO_2 evolution than Pt/anatase, with 443 µmol vs 413 µmol produced. Pt/rutile had the lowest CO_2 evolution at 134 µmol. It must be noted that gas evolution rate is dependent on the amount of catalyst in a non-linear fashion. Two competing factors influence this relationship, firstly the amount of active surface area of course increases with catalyst amount. However at higher catalyst loadings attenuation of light by the suspended photocatalyst becomes significant. Various other factors also contribute such as metal loading, stirring rate, and light intensity [27]. It has been shown elsewhere that a loading of around 1 mg/ml of catalyst is optimal [28] and therefore in this work this catalyst loading, the level of light excitation, and stirring rate were kept constant. The evolution of gas phase products over time are shown in Fig. S6. The H_2 evolution rate for each catalyst decreased slightly over the course of the reaction while the CO_2 evolution rate increased over the course of the reaction. The pH of reaction should also be considered as this will affect the partition of CO_2 between the liquid and gas phase.

The change in pH over time during the course of reaction is shown in Fig. S6. It can be seen that in all cases the pH decreases as the reaction proceeds primarily due to the formation of formic acid as a reaction intermediate. This decrease in pH over time results in an increase in CO_2 evolution and hence why the H_2/CO_2 ratio decreases over the course of the reaction for Pt/anatase and Pt/P25. The change in this ratio over time is shown in Fig. 2. In contrast, the CO_2 evolution slowed as the reaction progressed on Pt/rutile. Interestingly, the molar ratio of H_2 to CO_2 for Pt/P25 was almost exactly in the ratio of 2.5 after 4 h which would be expected from the stoichiometry of ethylene glycol photoreforming as shown in equation (2). However, Pt/anatase and Pt/rutile had molar ratios (H_2/CO_2) of 3.7 and 3.1, respectively after 4 h.

$$C_2H_6O_2 + 2H_2O \rightarrow 5H_2 + 2CO_2 \qquad (2)$$

This would indicate that over Pt/anatase a significant portion of the H_2 produced is derived from H_2O beyond the 2 mol that are expected per mole of ethylene glycol from the stoichiometry of (2) above. The "extra" protons required are likely to be derived from partial water oxidation in the proton coupled electron transfer reaction (3). The increased production of OH radicals then promotes the oxidation of ethylene glycol to glycolaldehyde resulting in even higher amount of protons available for reduction to H_2. Similar effects have been shown elsewhere by infrared spectroscopy where anatase was shown to be significantly more hydrophilic compared to P25 which affected the relative adsorption of alcohol and water [29].

$$H_2O + h^+ \rightarrow \bullet OH + H^+ \qquad (3)$$

In order to investigate the origin of the enhanced hydrogen production for the Pt/anatase catalyst the liquid phase products were analysed during the course of the reaction. As with the evolution of gaseous products, the conversion of ethylene glycol decreases with rutile content in the catalyst but this is a weak effect with conversions of 16.9 % for Pt/anatase, 16.7 % for Pt/P25, and 15.6 % for Pt/rutile after 4 h irradiation (Fig. 1). Interestingly when normalised to specific surface area of the support, the conversion over Pt/rutile is more efficient with 2821 µmol.m^{-2} of ethylene glycol converted after 4 h compared to 1581 µmol.m^{-2} and 1298 µmol.m^{-2} for Pt/P25 and Pt/anatase, respectively. The disparity in H_2 evolution rates and conversion may point towards differences in oxidation pathways taken by each catalyst. The concentrations of the carbon-containing intermediates and their selectivities over the course of the reaction are shown in Fig. 3. The selectivity towards glycolaldehyde during the course of the reaction follows the same trend as the H_2 production with Pt/anatase > Pt/P25 > Pt/rutile. Interestingly despite having the lowest conversion, Pt/rutile had the highest total amount of formaldehyde accumulated and consequently has the highest selectivity towards it. It should be noted that, as these are intermediate species in the oxidation of ethylene glycol, the amount of glycolaldehyde, formic acid, and formaldehyde present cannot be simply attributed to its rate of formation but is also determined by their rates of decomposition. Furthermore, in the case of formic acid, the presence of formates on the catalyst surface is likely to be significant, and therefore, its quantity in the liquid phase is not a complete picture.

3.2.2. Photoreforming of glycolaldehyde

As the first intermediate, the oxidation of glycolaldehyde is critical in determining the outcome of the overall reaction in ethylene glycol
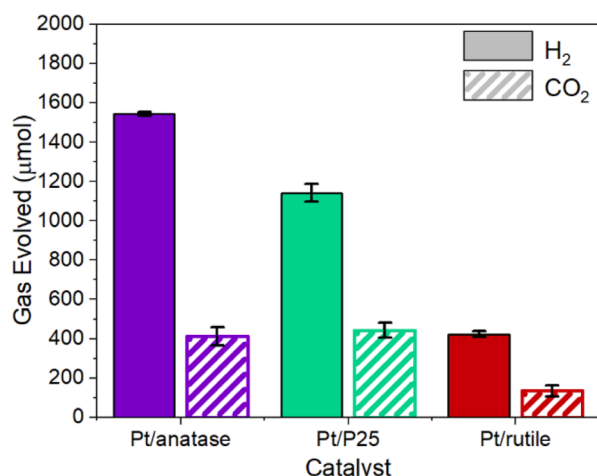
Table 1

Summary of characterisation results of synthesised Pt/TiO$_2$ catalysts.

Catalyst	Pt Loading (wt%)	Mean Pt Particle Diameter (nm)	Rutile Phase (wt%)	BET Surface Area (m^2/g)
Pt/anatase	0.22	0.43 ± 0.30	<1%	60.3
Pt/P25	0.23	0.59 ± 0.54*	19.6 %	40.4
Pt/rutile	0.19	0.65 ± 0.31	>99 %	21.2

Pt loading and particle diameter measured by ICP-OES and HAADF-STEM respectively. Rutile phase% calculated through relative XRD peak intensities. Surface area measured by N_2 Adsorption.
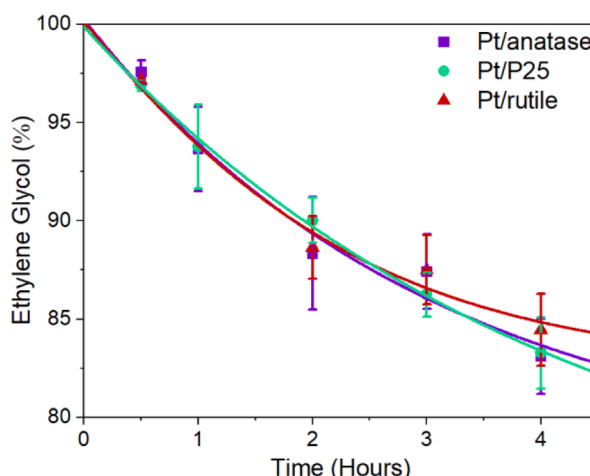*Particle size on anatase and rutile phases of P25 shown in Fig. S4.

Fig. 1. Total evolution of gas phase products and fractional conversion vs reaction time during the ethylene glycol photoreforming comparing Pt supported on anatase, rutile and TiO_2 P25. Reaction conditions: 40 mg catalyst, 40 ml of 0.3 M ethylene glycol aqueous solution, under UV irradiation for 4 h at ambient temperature.

Fig. 2. Molar ratio of H_2 to CO_2 during the photoreforming of ethylene glycol for different Pt/TiO_2 catalysts and theoretical ratio i.e. $5H_2 + 2CO_2$ (dotted line). Reaction conditions: 40 mg catalyst, 40 ml of 0.3 M ethylene glycol aqueous solution, under UV irradiation for 4 h at ambient temperature.

photoreforming. Therefore, photoreforming reactions were performed on glycolaldehyde as the starting material/sacrificial agent. In terms of gaseous phase products, the concentrations (Fig. S7) decreased in comparison to those during ethylene glycol photoreforming which is correlated with the lower conversion (Fig. 4). The H_2 evolution had decreased by 39.8 % (929 µmol. QE = 9.5 %), 27.4 % (892 µmol, QE = 8.5 %), and 26.6 % (312 µmol, QE = 3.2 %) for Pt/anatase, Pt/P25 and Pt/rutile respectively (Fig. 4). The evolution of H_2 followed the same trend as in ethylene glycol photoreforming, decreasing with the increasing rutile content of the catalyst. Similarly, the CO_2 evolution was slightly higher for Pt/P25 (281 µmol) in comparison to Pt/anatase (248 µmol) and both were higher than Pt/rutile (48 µmol). Small amounts of CO were observed on Pt/anatase which are likely to have been formed through the decarbonylation of the intermediate aldehydes or dehydration of formic acid [26,30,31]. The $H_2:CO_2$ ratio is shown in Fig. S7. Compared to ethylene glycol photoreforming, the Pt/anatase has a significantly lower ratio $H_2:CO_2$ during the glycolaldehyde photoreforming reaction. This highlights that the reason for the high initial activity for anatase towards ethylene glycol was due to its ability to produce high quantities of hydroxyl radicals. The oxidation of

glycolaldehyde is known to proceed via a direct hole transfer mechanism [32] and, therefore, this property of anatase is no longer as important. Pt/rutile has the highest $H_2:CO_2$ ratio due its poor reactivity towards glycolaldehyde and, therefore, poor conversion to CO_2.

The concentrations of the carbon-containing products and their selectivities for each catalyst over the course of the reaction are shown in Fig. 5. The Pt/rutile catalyst resulted in the lowest conversion (14.0 %) but in contrast to the ethylene glycol photoreforming now gave the lowest concentrations of formaldehyde and formic acid. The formaldehyde selectivity having decreased significantly from 66.7 % to 36.2 % after 4 h of irradiation (Fig. 5(e)). When the anatase and P25 based catalysts are compared both exhibit comparable conversion of glycolaldehyde at 17.2 % and 18.7 %, respectively, after 4 h of irradiation. In terms of selectivity towards the intermediates and CO_2 they both have similar profiles (Fig. 5(c)(d)). However in absolute concentrations the Pt/P25 had lower quantities of formic acid and formaldehyde formed (Fig. 5(a)(b)). This finding coupled with the higher CO_2 evolution clearly indicates that Pt/P25 is more active towards the conversion of the C1 species than Pt/anatase.
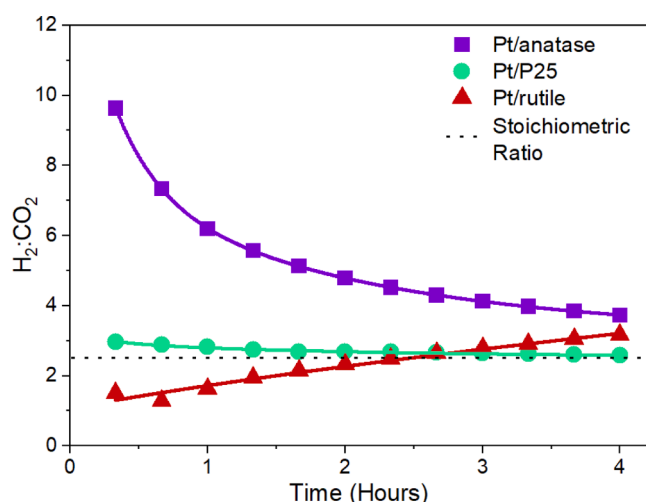
3.2.3. Photoreforming of formaldehyde

The formation of formaldehyde as a reaction intermediate in the photoreforming of ethylene glycol on Pt/TiO_2 appears to be crucial in determining the mineralisation rate and hence H_2 evolution. In particular there appears to be a strong dependence on the TiO_2 polymorph (Figs. 1 and 2). Therefore, photoreforming experiments were performed on formaldehyde using rutile, anatase and P25 TiO_2 based catalysts.

The Pt/P25 catalyst had the highest amount of H_2 and CO_2 evolved after 2 h with 173 µmol and 132 µmol, respectively. Pt/anatase had lower amounts of gas phase products with 74 µmol and 56 µmol H_2 and CO_2 produced. However, Pt/rutile produced almost zero gas phase products with < 5 µmol of each evolved after 2 h of photoreforming (Fig. S8). This is further highlighted by the conversion of formaldehyde as shown in Fig. 6. Pt/P25 had converted the most formaldehyde (88 %), followed by Pt/anatase (53 %), and the lowest conversion was found with Pt/rutile (15 %). Despite having converted some formaldehyde, Pt/rutile produced almost no CO_2 (Fig. S8). These results suggest that the reason for the lower H_2 evolution for Pt/rutile during ethylene glycol photoreforming may be due to its inability to oxidise the formaldehyde intermediate. This poor activity towards carbonyl groups over rutile based catalysts has been explored elsewhere for the selective production of aldehydes or ketones from alcohols where oxidation does not proceed past the desired carbonyl product [33–35]. This also explains the increase in $H_2:CO_2$ ratio over Pt/rutile as H_2 can be continually produced
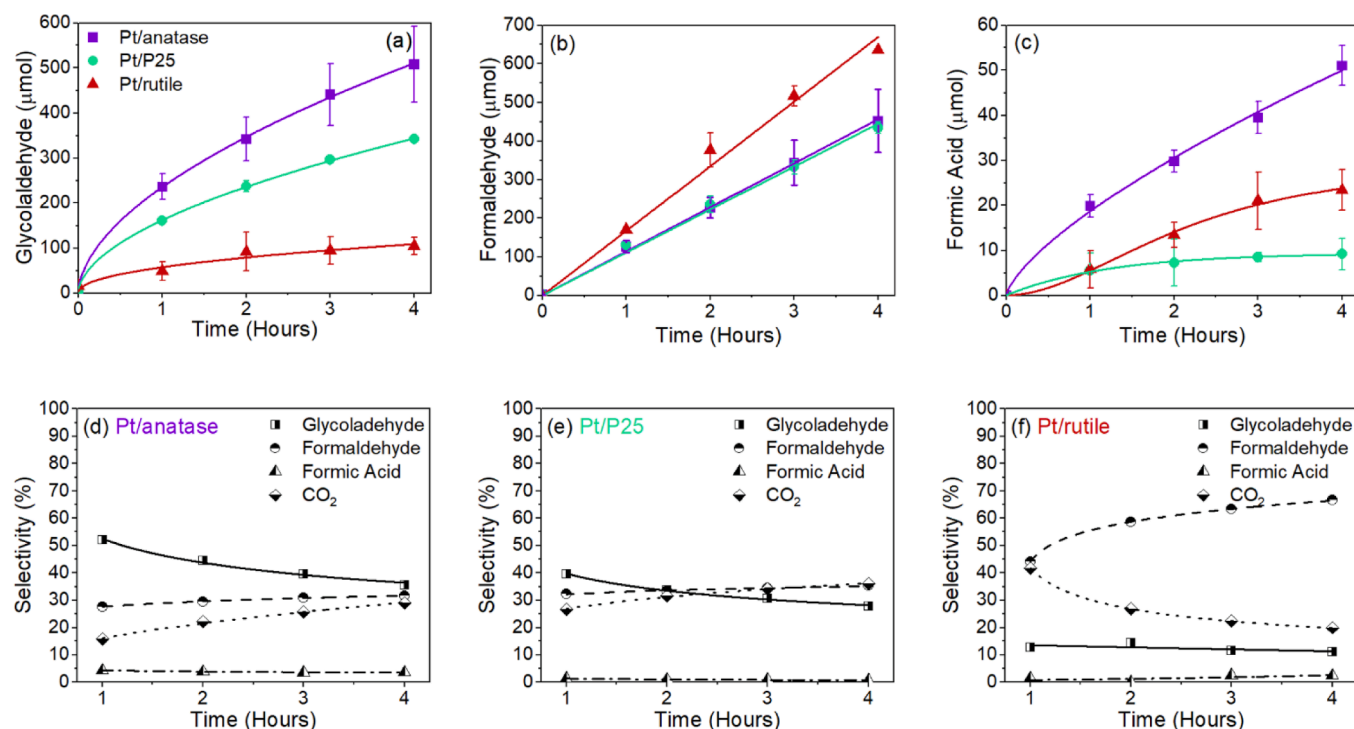
Fig. 3. Concentrations (a-c) of the different carbon-containing intermediates and their selectivities (d-f) over the course of the photoreforming of ethylene glycol reaction. Reaction conditions: 40 mg catalyst, 40 ml of 0.3 M ethylene glycol aqueous solution, under UV irradiation for 4 h at ambient temperature.
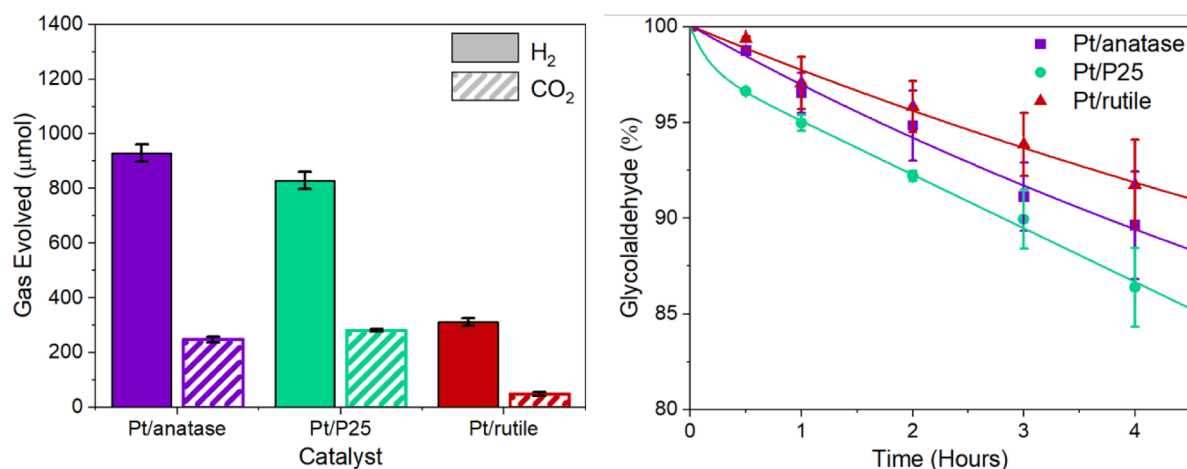

Fig. 4. Evolution rates of gas phase products and fractional conversion vs reaction time during the glycolaldehyde photoreforming comparing Pt supported on anatase, rutile and TiO_2 P25. Reaction conditions: 40 mg catalyst, 40 ml of 0.3 M glycolaldehyde aqueous solution, under UV irradiation for 4 h at ambient temperature.

as ethylene glycol is oxidised to formaldehyde but then CO_2 production is limited.

3.2.4. Oxidation pathway in ethylene glycol photoreforming over Pt/TiO_2

Oxidation pathways for each catalyst in the photoreforming of ethylene glycol can been proposed based on the presented quantitative analysis of gas and liquid phase products. Over Pt/rutile, the reaction is thought to primarily occur via the oxidation pathway (1) (Scheme 1) where ethylene glycol is split directly into two equivalents of formaldehyde, which then do not react further to produce formic acid. As can be seen from (1) only two H^+ per ethylene glycol molecule are released which explains the low H_2 evolution on Pt/rutile. However, a small proportion of the ethylene glycol is converted via glycolaldehyde as shown in (2). In contrast, Pt/anatase and Pt/P25 both primarily oxidise

glycolaldehyde via pathway (2) which results in full mineralisation. In this pathway ten H^+ are released per molecule of ethylene glycol resulting in a high H_2 evolution for Pt/anatase and Pt/P25.

In this work we have worked at a relatively high concentration of the initial substrate (0.3 M ethylene glycol), which may affect the selectivity towards different products. For example intermediates that have a much lower adsorption constant than ethylene glycol may not be oxidised as efficiently. It has been suggested that this is the case with formaldehyde [26]. We demonstrate this in Fig. 7 over Pt/P25. When a low concentration of ethylene glycol (2 mM) was used and when its conversion reaches around 30 % the formaldehyde concentration begins to decrease. At this point the surface coverage of ethylene glycol becomes low enough to enable the formaldehyde to adsorb. Acetic acid was also observed in this reaction which was not observed in the reactions at high
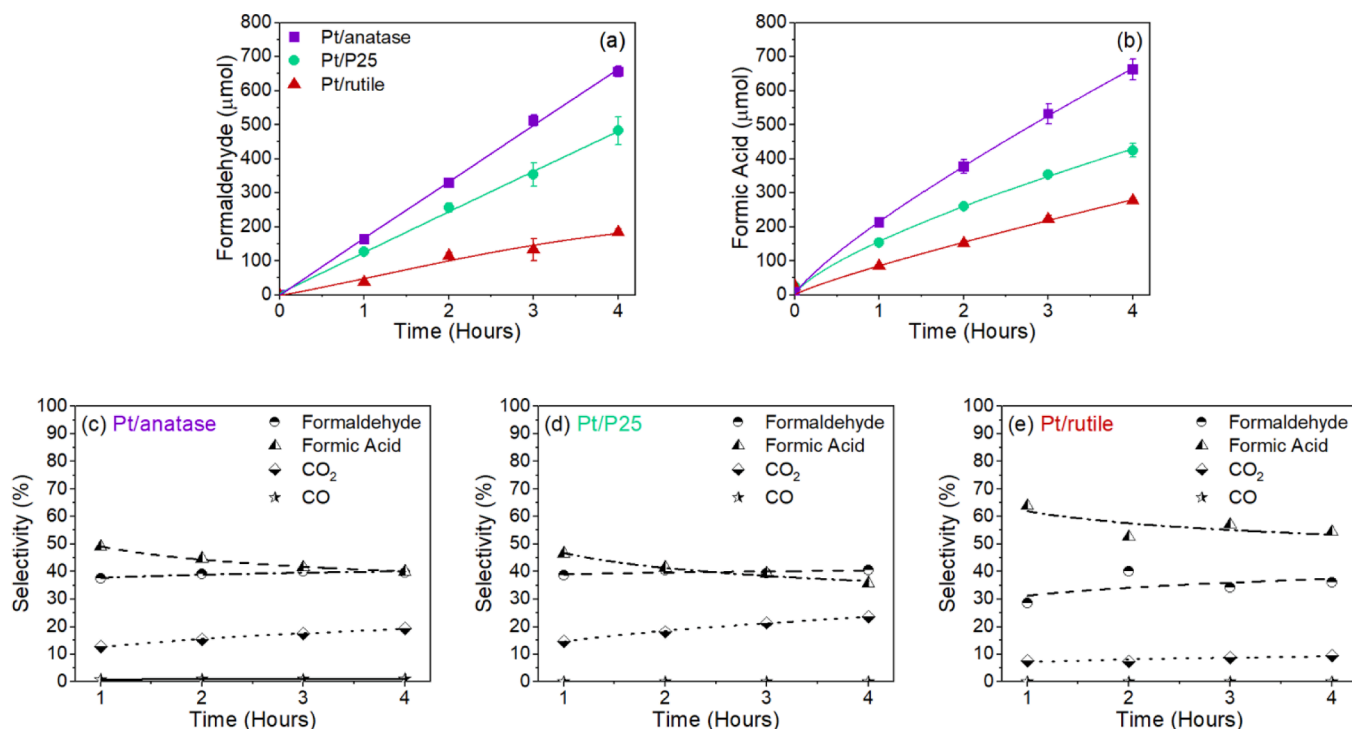
Fig. 5. Concentrations (a-b) of the different carbon-containing intermediates and their selectivities (c-e) over the course of the photoreforming of glycolaldehyde reaction.. Reaction conditions: 40 mg catalyst, 40 ml of 0.3 M glycolaldehyde aqueous solution, under UV irradiation for 4 h at ambient temperature.
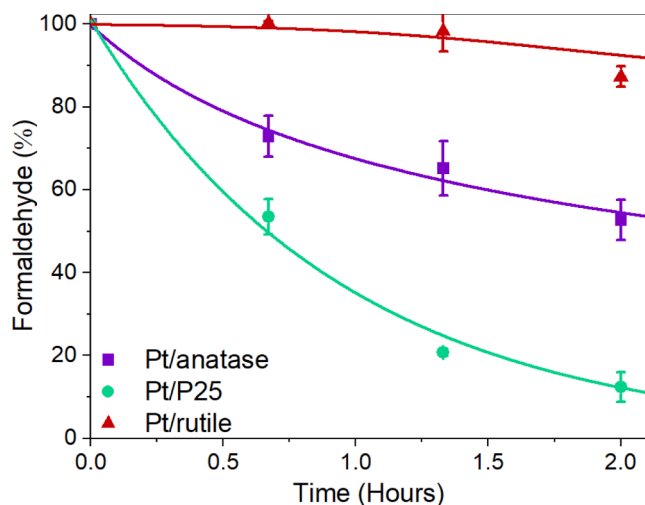

Fig. 6. Fractional conversion of formaldehyde during the photoreforming reaction comparing Pt supported on anatase, rutile and TiO_2 P25. Reaction conditions: 40 mg catalyst, 40 ml of 2 mM formaldehyde aqueous solution, under UV irradiation for 2 h at ambient temperature.

concentrations. This shows that dehydration pathways that have been reported elsewhere may only occur with low ethylene glycol surface coverages [26].

### 3.3. Oxidation mechanisms in ethylene glycol photoreforming

The variation in liquid phase intermediates between each catalyst shows that the H_2 evolution is not simply attributed to the activity of catalysts towards ethylene glycol but due to different oxidation pathways being favoured. The formation of formaldehyde appears to be related to the lower H_2 evolution particularly with Pt/rutile. The slow reactivity of formaldehyde limits the complete oxidation and therefore

limits the H_2 and CO_2 evolution. The oxidation reactions in the photoreforming of polyols have previously been shown to occur via two main mechanisms [26,32,36]. Briefly the two mechanisms can be described as follows:

Indirect (via Hydroxyl Radical) Pathway: oxidation is initiated by the abstraction of a hydrogen in the α-position to the oxygen moiety from molecules in close proximity to the catalyst surface by hydroxyl radicals. A water molecule is formed and the resulting carbon-centred radical combines with another hydroxyl radical or the radical electron is injected into the conduction band of the photocatalyst in a process known as current doubling. This leads to the sacrificial agent being converted to a more oxidised species of the same chain length analogous to Fenton's reagent chemistry [37], e.g. the conversion of ethylene glycol to glycolaldehyde.

Direct Hole Transfer Pathway: following dissociative chemisorption of the sacrificial agent on the catalyst surface, a hole is transferred directly leading to the formation of an alkoxy radical and subsequent cleavage of the adjacent C–C bond and the release of C1 species. As a general rule, hydroxyl groups release formaldehyde, aldehyde groups release formic acid, and acid groups release CO_2.

In-situ spectroscopic studies on ethylene glycol and glycerol have revealed some insight into the factors that influence the relative importance of each oxidation mechanism. Li *et al.* first showed that oxidative C–C cleavage occurs over P25 based catalysts, however, this was under aerobic conditions and therefore the role of superoxide radicals is likely to be significant [38]. Lv *et al.* investigated the C–C cleavage of glycerol under anaerobic conditions using P25 based catalysts [39]. It was found that dissociation of the reactants was key in determining the degree of C–C cleavage although from this study it is still unclear how this depends on crystalline phase or at which stage of the reaction that this occurred i.e. glycerol or subsequent intermediates. Jin *et al.* found that oxidative C–C cleavage of ethylene glycol was the only pathway that occurred over rutile (110) surfaces in anaerobic conditions [40]. This finding is consistent with our results showing high selectivity towards formaldehyde over Pt/rutile. It also shows that some feature of the dominant rutile (110) facet is key in promoting oxidative
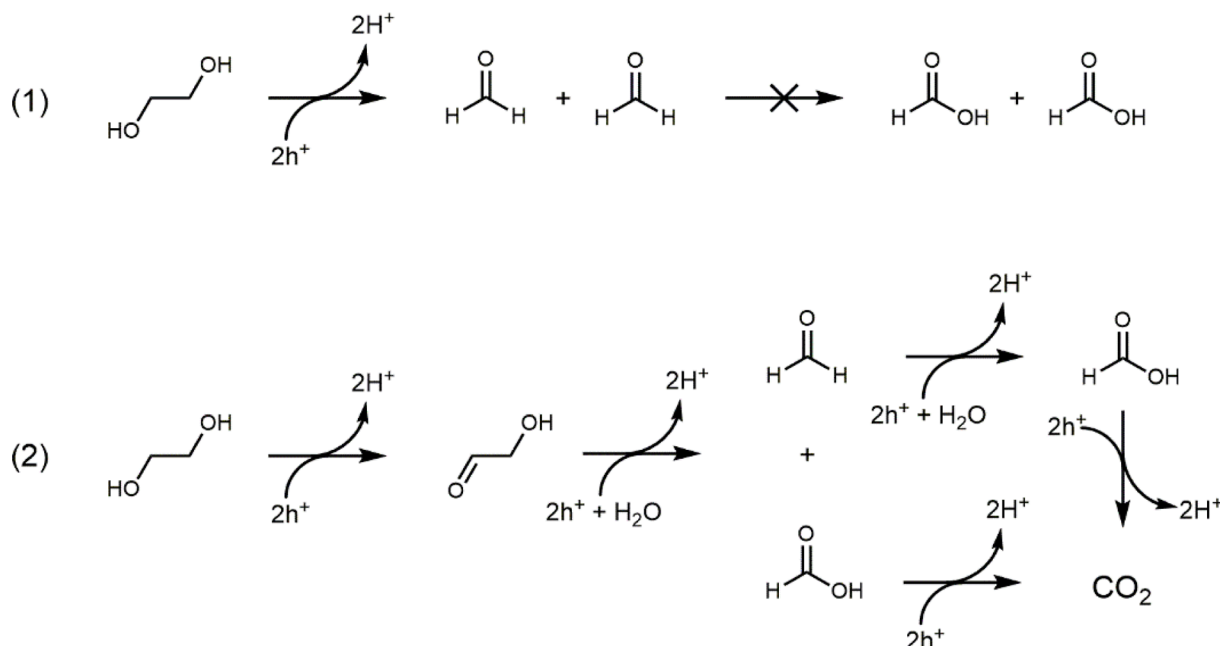
Scheme 1. Proposed oxidation pathways for ethylene glycol photoreforming. Pt/rutile primarily follows pathway (1) whereas Pt/anatase and Pt/P25 primarily follow pathway (2).
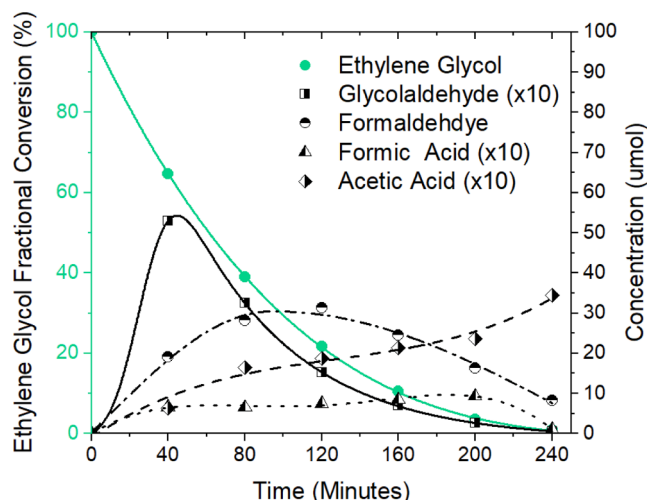

Fig. 7. Conversion of ethylene glycol (left y axis) and concentration of liquid phase intermediates (right y axis) from the photoreforming of ethylene glycol over Pt/P25 at low concentration. Reaction conditions: 40 mg catalyst, 40 ml of 2 mM ethylene glycol aqueous solution, under UV irradiation for 2 h at ambient temperature.

C–C cleavage whereas other exposed facets may result in the hydroxyl radical mediated route to glycolaldehyde. Previous reports have shown alcohols to only dissociatively adsorb on rutile whereas a mix of chemi- and physisorbed alcohol was found to occur on anatase [41]. Combined with the two possible oxidation mechanisms, this serves as an explanation why different oxidation pathways are observed on TiO$_2$ with different phase compositions. Therefore, it is proposed that the indirect hydroxyl radical driven mechanism is dominant on anatase containing catalysts (Pt/anatase and Pt/P25) whereas the direct hole transfer mechanism is dominant on rutile. As shown in Scheme 2 below, the conversion of ethylene glycol to glycolaldehyde can be easily described by the indirect mechanism (1). This is clearly seen as Pt/anatase had the greatest selectivity towards glycolaldehyde in the photoreforming reactions. Furthermore, it has been shown previously that anatase

produces much greater quantities of hydroxyl radicals than rutile [15] which supports this hypothesis. In contrast, the high selectivity towards formaldehyde during ethylene glycol photoreforming indicates that the rutile-based catalyst is active towards the direct C–C bond cleavage of ethylene glycol as shown in Scheme 2 (2) with only a small amount being oxidised via glycolaldehyde. The decreased selectivity towards formaldehyde during glycolaldehyde photoreforming further supports the proposal that ethylene glycol is mainly directly split into two equivalents of formaldehyde on the rutile catalyst. It has been suggested previously that peroxo- Ti-O-O-Ti species formed on rutile surfaces are responsible for C–C cleavage in glycerol and glucose photoreforming [3,21]. The more mildly oxidising peroxo- species is formed through the coupling of adjacent surface hydroxyl radicals exclusively on the rutile surface [42]. However, we believe that the oxidation behaviour on rutile is more simply explained by ethylene glycol preferring to dissociatively adsorb on rutile leading to the direct hole transfer mechanism shown in (2) below. Vicinal diols have been computed to bridge coordinatively unsaturated Ti$_{5C}$ sites which are prevalent on the dominant (110) facet of rutile [43] in a bidentate fashion [44,45]. In fact, this adsorption behaviour of ethylene glycol has been employed to cap the (110) facet by complexation to Ti in the synthesis of rutile nanorods [46]. This is in contrast to the behaviour of mono-alcohols on rutile where chemisorption leads abstraction of an α-hydrogen and oxidation to the corresponding carbonyl compound without C–C cleavage [47,48]. Peroxo- species may play a role in these cases, yet on the basis of this work it appears that on poly-alcohols direct hole-transfer mechanisms prevail. The formation of peroxo- species, however, may in part explain the lack of mobile hydroxyl radicals on rutile. This may be why our results show only a little ethylene glycol is converted to glycolaldehyde on Pt/rutile which is a hydroxyl radical driven process. This may also explain why Pt/rutile is unable to covert formaldehyde as oxidation to formic acid also requires hydroxyl radicals [49].

For P25 it has been widely reported that synergistic effects of the two phases result in a higher reaction rate compared to pure phases due to enhanced charge separation, however this has been disputed. Wahab et al. have suggested that the enhancement results from a lattice expansion in the anatase crystallite which increases its photocatalytic performance [28]. Our results suggest that, in-part, the advantage of having a mixture of anatase and rutile phases is an additive one in terms
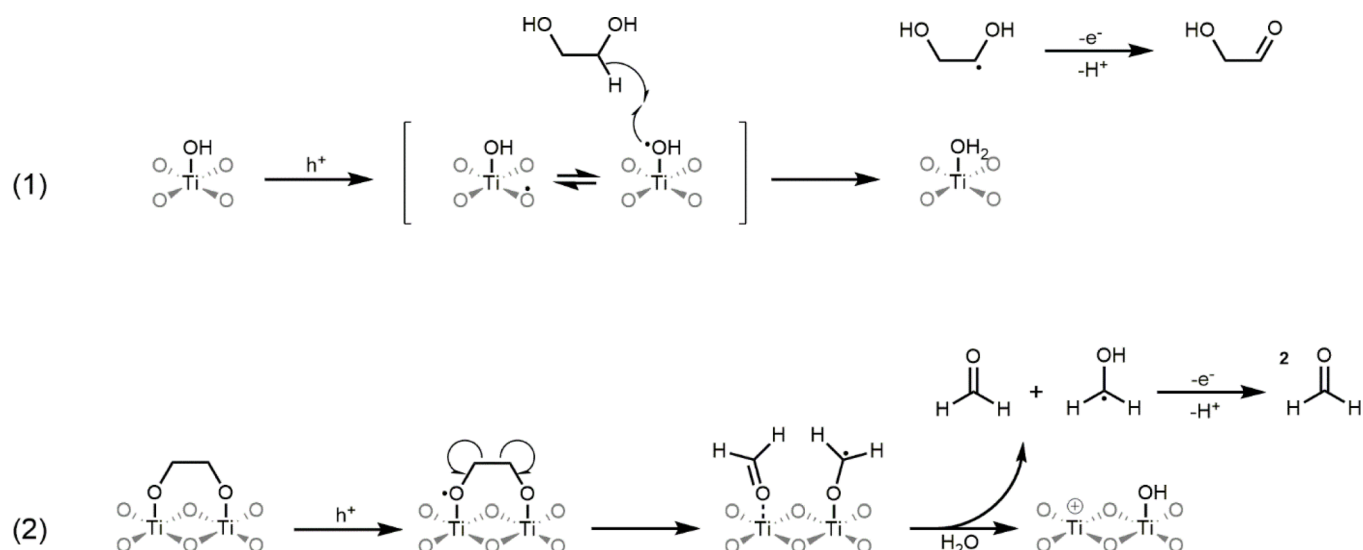
Scheme 2. Proposed primary oxidation mechanisms for ethylene glycol (0.3 M) photoreforming over Pt/TiO$_2$.(1) Indirect hole transfer via hydroxyl radicals resulting in glycolaldehyde over Pt/anatase and Pt/P25. (2) Direct hole transfer: ethylene glycol is converted to two equivalents of formaldehyde (C–C cleavage) which is subsequently unable to undergo further oxidation over Pt/rutile.

of oxidation mechanisms. It is able to convert ethylene glycol to glycolaldehyde and formaldehyde to formic acid via the hydroxyl driven mechanism efficiently. However, it is also efficient at the C–C cleavage type mechanisms such as the conversion of glycolaldehyde. This does mean also that a proportion of ethylene glycol may be split directly into formaldehyde on Pt/P25 as it is on Pt/rutile. Importantly, this does not hinder the gas evolution, as is the case with pure rutile, as it is also able to convert formaldehyde efficiently. This ability of mixed phase TiO$_2$ to efficiently perform both oxidation mechanisms may serve as one explanation for it's often reported high activity. As different intermediates are oxidised via the different mechanisms, a mixed phase catalyst prevents a buildup of certain compounds in the liquid phase leading to more effective mineralization to CO$_2$.

4. Conclusions

The photoreforming of ethylene glycol over 0.2 wt% Pt/TiO$_2$ photocatalysts was found to have significant dependence on the specific titania polymorph used. Pt/anatase was the most active catalyst with an H$_2$ evolution of 1543 μmol vs Pt/P25 and Pt/rutile with 1142 and 423 μmol respectively. However when surface area was considered Pt/P25 had higher specific H$_2$ evolution than Pt/anatase. The differences in H$_2$ evolution were found to be a result of difference in oxidation pathway taken by each catalyst. Pt/rutile with the lowest H$_2$ evolution was found to preferentially convert ethylene glycol directly into two equivalents of formaldehyde. Pt/rutile was then unable to covert the formaldehyde produced effectively and it largely accumulates in the liquid phase limiting the amount of H$_2$ produced. Pt/anatase and Pt/P25 both oxidised ethylene glycol via glycolaldehyde prior to C–C cleavage and subsequent full oxidation to CO$_2$ and, therefore, produce higher quantities of H$_2$. The differences in oxidation pathway can be explained in terms of adsorption and hole transfer mechanism. Over Pt/anatase and Pt/P25 the dominant mechanism for ethylene glycol oxidation is an indirect hole transfer and hydrogen abstraction yielding glycolaldehyde. However, over Pt/rutile direct hole transfer to surface complexed ethylene glycol results in oxidative C–C cleavage to formaldehyde. Pt/P25 was found to be more effective towards the degradation of formaldehyde and formic acid. Overall, Pt/anatase and Pt/P25 oxidised ethylene glycol to CO$_2$ at similar rates despite difference in the rates towards the intermediate species. It has been shown before that the TiO$_2$ polymorph affects the H$_2$ evolution rate in ethylene glycol

photoreforming [50]. However, herein, we have shown the reasons for this are far more complex than being simply due to the different charge carrier dynamics of the respective polymorphs. While being unfavourable in terms of H$_2$ production in this work, rutile based catalysts may perform better when more complex substrates are used due to its ability to cleave C–C bonds of glycol groups efficiently. These results may also be of benefit to the research area of partial photo-oxidation to value added products where selectivity over oxidation products is essential.

CRediT authorship contribution statement

Luke Roebuck: Writing – review & editing, Writing – original draft, Investigation, Formal analysis, Data curation, Conceptualization. **Helen Daly:** Writing – review & editing, Validation, Supervision, Investigation. **Lan Lan:** Writing – review & editing, Investigation. **Joseph Parker:** Writing – review & editing, Investigation, Formal analysis, Data curation. **Angus Gostick:** Investigation. **Nathan Skillen:** Writing – review & editing, Resources. **Sarah J. Haigh:** Writing – review & editing, Supervision, Methodology, Investigation. **Marta Falkowska:** Writing – review & editing, Supervision. **Christopher Hardacre:** Writing – review & editing, Supervision, Project administration, Funding acquisition, Conceptualization.

Declaration of competing interest

The authors declare that they have no known competing financial interests or personal relationships that could have appeared to influence the work reported in this paper.

Acknowledgements

Appendix A. Supplementary data

Supplementary data to this article can be found online at https://doi.org/10.1016/j.jcat.2024.115876

Data availability

Open access data is available at https://doi.org/10.48420/27954024.

References

[1] H. Bahruji, M. Bowker, P.R. Davies, J. Kennedy, D.J. Morgan, The importance of metal reducibility for the photo-reforming of methanol on transition metal-TiO₂ photocatalysts and the use of non-precious metals, Int. J. Hydrogen Energy 40 (2015) 1465–1471, https://doi.org/10.1016/j.ijhydene.2014.11.097.

[2] A.V. Puga, A. Forneli, H. García, A. Corma, Production of H₂ by Ethanol Photoreforming on Au/TiO₂, Adv. Funct. Mater. 24 (2014) 241–248, https://doi.org/10.1002/adfm.201301907.

[3] M. Bellardita, E.I. García-López, G. Marcì, L. Palmisano, Photocatalytic formation of H₂ and value-added chemicals in aqueous glucose (Pt)-TiO₂ suspension, Int. J. Hydrogen Energy 41 (2016) 5934–5947, https://doi.org/10.1016/j.ijhydene.2016.02.103.

[4] L. Lan, H. Daly, Y. Jiao, Y. Yan, C. Hardacre, X. Fan, Comparative study of the effect of TiO₂ support composition and Pt loading on the performance of Pt/TiO₂ photocatalysts for catalytic photoreforming of cellulose, Int. J. Hydrogen Energy 46 (2021) 31054–31066, https://doi.org/10.1016/j.ijhydene.2021.06.043.

[5] T. Uekert, M.F. Kuehnel, D.W. Wakerley, E. Reisner, Plastic waste as a feedstock for solar-driven H₂ generation, Energy Environ. Sci. 11 (2018) 2853–2857, https://doi.org/10.1039/C8EE01408F.

[6] M. Bowker, H. Bahruji, J. Kennedy, W. Jones, G. Hartley, C. Morton, The Photocatalytic Window: Photo-Reforming of Organics and Water Splitting for Sustainable Hydrogen Production, Catal. Lett. 145 (2015) 214–219, https://doi.org/10.1007/s10562-014-1443-x.

[7] A. Malik, M. Lenzen, A. Geschke, Triple bottom line study of a lignocellulosic biofuel industry, Glob. Change Biol. Bioenergy 8 (2016) 96–110, https://doi.org/10.1111/gcbb.12240.

[8] S.Y. Toledo-Camacho, S. Contreras Iglesias, Photocatalytic Hydrogen Production from Waste, in: Photocatalytic Hydrogen Production for Sustainable Energy, 2023, pp. 245-273.

[9] E. Barnard, J.J. Rubio Arias, W. Thielemans, Chemolytic depolymerisation of PET: a review, Green Chem. 23 (2021) 3765–3789, https://doi.org/10.1039/D1GC00887K.

[10] H. Warsahartana, A. Basir, A. Keyworth, R. Davis, M. Falkowska, E. Asuquo, S. Edmondson, A. Garforth, Catalytic Steam Hydrolysis of Polyethylene Terephthalate to Terephthalic Acid followed by Repolymerisation, Chem. Eng. Trans. 100 (2023) 445–450, https://doi.org/10.3303/CET23100075.

[11] D.P. Davis, K.J. Bramwell, R.S. Hamilton, S.R. Williams, Ethylene glycol poisoning: case report of a record-high level and a review, J. Emerg. Med. 15 (1997) 653–667, https://doi.org/10.1016/s0736-4679(97)00145-5.

[12] C.A. Staples, J.B. Williams, G.R. Craig, K.M. Roberts, Fate, effects and potential environmental risks of ethylene glycol: a review, Chemosphere 43 (2001) 377–383, https://doi.org/10.1016/s0045-6535(00)00148-x.

[13] A. Fujishima, K. Honda, Electrochemical Photolysis of Water at a Semiconductor Electrode, Nature 238 (1972) 37–38, https://doi.org/10.1038/238037a0.

[14] G. Odling, N. Robertson, Why is Anatase a Better Photocatalyst than Rutile? The Importance of Free Hydroxyl Radicals, ChemSusChem 8 (2015) 1838–1840, https://doi.org/10.1002/cssc.201500298.

[15] W. Kim, T. Tachikawa, G.-H. Moon, T. Majima, W. Choi, Molecular-Level Understanding of the Photocatalytic Activity Difference between Anatase and Rutile Nanoparticles, Angew. Chem. Int. Ed. 53 (2014) 14036–14041, https://doi.org/10.1002/anie.201406625.

[16] T. Luttrell, S. Halpegamage, J. Tao, A. Kramer, E. Sutter, M. Batzill, Why is anatase a better photocatalyst than rutile? - Model studies on epitaxial TiO₂ films, Sci. Rep. 4 (2014) 4043, https://doi.org/10.1038/srep04043.

[17] B. Ohtani, O.O. Prieto-Mahaney, D. Li, R. Abe, What is Degussa (Evonik) P25? Crystalline composition analysis, reconstruction from isolated pure particles and photocatalytic activity test, J. Photochem. Photobiol. A 216 (2010) 179–182, https://doi.org/10.1016/j.jphotochem.2010.07.024.

[18] P. Apopei, C. Catrinescu, C. Teodosiu, S. Royer, Mixed-phase TiO₂ photocatalysts: Crystalline phase isolation and reconstruction, characterization and photocatalytic activity in the oxidation of 4-chlorophenol from aqueous effluents, Appl. Catal. B Environ. 160–161 (2014) 374–382, https://doi.org/10.1016/j.apcatb.2014.05.030.

[19] S. Cong, Y. Xu, Explaining the High Photocatalytic Activity of a Mixed Phase TiO₂: A Combined Effect of O₂ and Crystallinity, J. Phys. Chem. C 115 (2011) 21161–21168, https://doi.org/10.1021/jp2055206.

[20] V. Maslova, A. Fasolini, M. Offidani, S. Albonetti, F. Basile, Solar-driven valorization of glycerol towards production of chemicals and hydrogen, Catal. Today 380 (2021) 147–155, https://doi.org/10.1016/j.cattod.2021.03.008.

[21] R. Chong, J. Li, X. Zhou, Y. Ma, J. Yang, L. Huang, H. Han, F. Zhang, C. Li, Selective photocatalytic conversion of glycerol to hydroxyacetaldehyde in aqueous solution on facet tuned TiO₂-based catalysts, Chem. Comm. 50 (2014) 165–167, https://doi.org/10.1039/C3CC46515B.

[22] R. Chong, J. Li, Y. Ma, B. Zhang, H. Han, C. Li, Selective conversion of aqueous glucose to value-added sugar aldose on TiO₂-based photocatalysts, J. Catal. 314 (2014) 101–108, https://doi.org/10.1016/j.jcat.2014.03.009.

[23] A. Mills, M. Bingham, C. O'Rourke, M. Bowker, Modelled kinetics of the rate of hydrogen evolution as a function of metal catalyst loading in the photocatalysed reforming of methanol by Pt (or Pd)/TiO₂, J. Photochem. and Photobiol. A Chem. 373 (2019) 122–130, https://doi.org/10.1016/j.jphotochem.2018.12.039.

[24] R.A. Spurr, H. Myers, Quantitative Analysis of Anatase-Rutile Mixtures with an X-Ray Diffractometer, Anal. Chem. 29 (1957) 760–762, https://doi.org/10.1021/ac60125a006.

[25] V.M. Daskalaki, P. Panagiotopoulou, D.I. Kondarides, Production of peroxide species in Pt/TiO₂ suspensions under conditions of photocatalytic water splitting and glycerol photoreforming, Chem. Eng. J. 170 (2011) 433–439, https://doi.org/10.1016/j.cej.2010.11.093.

[26] T.F. Berto, K.E. Sanwald, W. Eisenreich, O.Y. Gutiérrez, J.A. Lercher, Photoreforming of ethylene glycol over Rh/TiO₂ and Rh/GaN:ZnO, J. Catal. 338 (2016) 68–81, https://doi.org/10.1016/j.jcat.2016.02.021.

[27] Y. Yao, Y. Zheng, Y. Yang, Numerical Simulation of Energy and Mass Transfer in a Magnetic Stirring Photocatalytic Reactor, in, Sustainability (2023).

[28] A.K. Wahab, S. Ould-Chikh, K. Meyer, H. Idriss, On the "possible" synergism of the different phases of TiO2 in photo-catalysis for hydrogen production, J. Catal. 352 (2017) 657–671, https://doi.org/10.1016/j.jcat.2017.04.033.

[29] V. Augugliaro, H. Kisch, V. Loddo, M.J. López-Muñoz, C. Márquez-Álvarez, G. Palmisano, L. Palmisano, F. Parrino, S. Yurdakal, Photocatalytic oxidation of aromatic alcohols to aldehydes in aqueous suspension of home prepared titanium dioxide: 2. Intrinsic and surface features of catalysts, Appl. Catal. A 349 (2008) 189–197, https://doi.org/10.1016/j.apcata.2008.07.038.

[30] J. Davis, M. Barteau, Polymerization and decarbonylation reactions of aldehydes on the Pd (111) surface, J. Am. Chem. Soc. 111 (1989) 1782–1792. https://doi.org/10.1021/ja00187a035.

[31] V.I. Avdeev, V.N. Parmon, Molecular Mechanism of the Formic Acid Decomposition on V₂O₅/TiO₂ Catalysts: A Periodic DFT Analysis, J. Phys. Chem. C 115 (2011) 21755–21762, https://doi.org/10.1021/jp204652n.

[32] K.E. Sanwald, T.F. Berto, W. Eisenreich, O.Y. Gutiérrez, J.A. Lercher, Catalytic routes and oxidation mechanisms in photoreforming of polyols, J. Catal. 344 (2016) 806–816, https://doi.org/10.1016/j.jcat.2016.08.009.

[33] S. Yurdakal, G. Palmisano, V. Loddo, V. Augugliaro, L. Palmisano, Nanostructured Rutile TiO₂ for Selective Photocatalytic Oxidation of Aromatic Alcohols to Aldehydes in Water, J. Am. Chem. Soc. 130 (2008) 1568–1569, https://doi.org/10.1021/ja709989e.

[34] D. Brinkley, T. Engel, Photocatalytic Dehydrogenation of 2-Propanol on TiO₂(110), J. Phys. Chem. B 102 (1998) 7596–7605, https://doi.org/10.1021/jp981901l.

[35] C.A. Walenta, C. Courtois, S.L. Kollmannsberger, M. Eder, M. Tschurl, U. Heiz, Surface Species in Photocatalytic Methanol Reforming on Pt/TiO₂(110): Learning from Surface Science Experiments for Catalytically Relevant Conditions, ACS Catal. 10 (2020) 4080–4091, https://doi.org/10.1021/acscatal.0c00260.

[36] C. Minero, A. Bedini, V. Maurino, Glycerol as a probe molecule to uncover oxidation mechanism in photocatalysis, Appl. Catal. B 128 (2012) 135–143, https://doi.org/10.1016/j.apcatb.2012.02.014.

[37] B. Dietrick McGinnis, V. Dean Adams, E. Joe Middlebrooks, Degradation of ethylene glycol using Fenton's reagent and UV, Chemosphere 45 (2001) 101–108, https://doi.org/10.1016/S0045-6535(00)00597-X.

[38] C. Li, X. Wang, A. Cheruvathur, Y. Shen, H. Xiang, Y. Li, J.W. Niemantsverdriet, R. Su, In-situ probing photocatalytic C-C bond cleavage in ethylene glycol under ambient conditions and the effect of metal cocatalyst, J. Catal. 365 (2018) 313–319, https://doi.org/10.1016/j.jcat.2018.07.017.

[39] D. Lv, Y. Lei, D. Zhang, X. Song, Y.W. Li, J.W.H. Niemantsverdriet, W. Hao, Y. Deng, R. Su, Effect of Pd and Au on Hydrogen Abstraction and C-C Cleavage in Photoconversion of Glycerol: Beyond Charge Separation, J. Phys. Chem. C 124 (2020) 20320–20327, https://doi.org/10.1021/acs.jpcc.0c07148.

[40] X. Jin, C. Li, C. Xu, D. Guan, A. Cheruvathur, Y. Wang, J. Xu, D. Wei, H. Xiang, J. W. Niemantsverdriet, Y. Li, Q. Guo, Z. Ma, R. Su, X. Yang, Photocatalytic C-C bond cleavage in ethylene glycol on TiO₂: A molecular level picture and the effect of metal nanoparticles, J. Catal. 354 (2017) 37–45, https://doi.org/10.1016/j.jcat.2017.08.004.

[41] G. Ramis, G. Busca, V. Lorenzelli, Structural effects on the adsorption of alcohols on titanium dioxides, J. Chem. Soc., Faraday Trans. 1 83 (1987) 1591-1599. DOI: 10.1039/F19878301591.

[42] J. Zhang, Y. Nosaka, Mechanism of the OH Radical Generation in Photocatalysis with TiO₂ of Different Crystalline Types, J. Phys. Chem. C 118 (2014) 10824–10832, https://doi.org/10.1021/jp501214m.

[43] M. Ramamoorthy, D. Vanderbilt, R.D. King-Smith, First-principles calculations of the energetics of stoichiometric TiO₂ surfaces, PhysRevB 49 (1994) 16721–16727, https://doi.org/10.1103/PhysRevB.49.16721.

[44] C. Rohmann, H. Idriss, A computational study of the interaction of oxygenates with the surface of rutile TiO$_2$(110). Structural and electronic trends, J. Phys.: Condens. Matter 34 (2022) 154002, https://doi.org/10.1088/1361-648X/ac4d5b.

[45] G. Carchini, N. López, Adsorption of small mono- and poly-alcohols on rutile TiO$_2$: a density functional theory study, Phys. Chem. Chem. Phys. 16 (2014) 14750–14760, https://doi.org/10.1039/C4CP01546K.

[46] C. Xiong, X. Deng, J. Li, Preparation and photodegradation activity of high aspect ratio rutile TiO$_2$ single crystal nanorods, Appl. Catal. b: Environ. 94 (2010) 234–240, https://doi.org/10.1016/j.apcatb.2009.11.013.

[47] S.L. Kollmannsberger, C.A. Walenta, C. Courtois, M. Tschurl, U. Heiz, Thermal Control of Selectivity in Photocatalytic, Water-Free Alcohol Photoreforming, ACS Catal. 8 (2018) 11076–11084, https://doi.org/10.1021/acscatal.8b03479.

[48] J.Ø. Hansen, R. Bebensee, U. Martinez, S. Porsgaard, E. Lira, Y. Wei, L. Lammich, Z. Li, H. Idriss, F. Besenbacher, B. Hammer, S. Wendt, Unravelling Site-Specific Photo-Reactions of Ethanol on Rutile TiO$_2$(110), Sci. Rep. 6 (2016) 21990, https://doi.org/10.1038/srep21990.

[49] H. Belhadj, S. Hamid, P.K.J. Robertson, D.W. Bahnemann, Mechanisms of Simultaneous Hydrogen Production and Formaldehyde Oxidation in H$_2$O and D$_2$O over Platinized TiO$_2$, ACS Catal. 7 (2017) 4753–4758, https://doi.org/10.1021/acscatal.7b01312.

[50] W.-T. Chen, A. Chan, Z.H.N. Al-Azri, A.G. Dosado, M.A. Nadeem, D. Sun-Waterhouse, H. Idriss, G.I.N. Waterhouse, Effect of TiO$_2$ polymorph and alcohol sacrificial agent on the activity of Au/TiO$_2$ photocatalysts for H$_2$ production in alcohol–water mixtures, J. Catal. 329 (2015) 499–513, https://doi.org/10.1016/j.jcat.2015.06.014.